TEMPERATURE DEPENDENT ELECTROCHEMICAL CO_2 REDUCTION REACTION ON POLYCRYSTALLINE COPPER AND MANGANESE OXIDE

A Thesis

Presented to the Faculty of the Graduate School

of Cornell University

In Partial Fulfillment of the Requirements for the Degree of

Master of Science

by

Yixu Zong

August 2019

ABSTRACT

The electrochemical CO_2 reduction reaction (CO_2RR) has caught researchers' attention over the past decades because of its potential for sustainable energy storage and conversion. In the previous research, copper has been discovered as a valuable catalyst based on its excellence in converting CO_2 to higher-order hydrocarbons. Different from most of the work focusing on the room temperature (~25^{o}C), we investigate CO_2RR on polycrystalline copper electrode under lower (5^{o}C, 15^{o}C) and higher (35^{o}C, 45^{o}C) temperatures across a range of potentials to observe the shift in the reaction selectivity toward each major gaseous product, CH_4, C_2H_4, CO, and H_2. By making Arrhenius plots, we can analyze the thermodynamic parameter (activation energy, E_a) per product at each studied potential and discuss the underlying mechanism with the change of the reaction temperature. This temperature dependent experiment also involves a custom-designed electrochemical cell, which can be simply applied to the electrochemical test on other potential CO_2RR catalysts. Therefore, using this custom design with the fundamental understanding of the temperature dependent CO_2RR mechanism, we select Mn_3O_4 nanocrystals (NCs) to keep studying the temperature effect of CO_2RR as well as explore the efficient post-synthetic surface cleaning methods, among thermal, alkylation, Lewis-acid, and base treatment, by comparing electrochemical analysis and physical characterizations. From our results, even though Mn_3O_4 NCs are not good materials for CO_2RR, we could conclude that alkylation treatment is the most efficient way to remove the surface ligands from the Arrhenius analysis.

BIOGRAPHICAL SKETCH

Yixu Zong is a Master of Science student in Professor Jin Suntivich's group in the Department of Materials Science and Engineering at Cornell University. Her research focuses on anion exchange of sulfide on the electrochemical activity of manganese oxide. She is currently investigating temperature dependent CO2 reduction on copper to gain insights into the possible similar experiment on manganese oxide and oxysulfide in the future.

Yixu was born and grew up in Harbin, China. She began her study in the US in 2012 and received her bachelor's degree in chemistry with a certificate in German from University of Wisconsin-Madison in 2017. In Wisconsin, she worked in the field of chemical vapor deposition synthesis and temperature-dependent UV-Visible spectroscopic characterization of transition metal dichalcogenides.

During Yixu's undergraduate study, she also visited University of Science and Technology, China as a visiting Undergraduate Research assistant where she performed research on the influence of annealed temperature on the electrochemical activity of copper porphyrin conjugated microporous polymers.

ACKNOWLEDGMENTS

The temperature dependent CO2 redcution work was supported by the National Science Foundation (NSF) under Grant No. CHE-1665305. The manganese nanocrystals related research was funded by NSF (CHE-1805400). I would like to thank Professor Jin Suntivich, Professor Francis DiSalvo, and Professor Richard Robinson at Cornell University for the support of my MS thesis research. Also, I would thank Andrew Nelson, PhD from Professor Robinson group for the synthesis and physical characterization of manganese oxide nanocrystals.

TABLE OF CONTENTS

VOLUME I: TEMPERATURE DEPENDENT ELECTROCHEMICAL CO_2 REDUCTION REACTION ON POLYCRYSTALLINE COPPER

I. Introduction

To address the increasingly severe Earth's climate concern, the reduction of carbon dioxide (CO_2) in the atmosphere is an important mission for both academic and industrial researchers.[1] Electrochemical CO_2 reduction (CO_2RR) has the potential to convert CO_2 to high-valued carbon products, such as CO and hydrocarbons, at relatively low temperature.[2, 3] Thus far, polycrystalline copper is one of the most promising catalysts because of its ability to produce a significant amount of hydrocarbons.[4, 5] However, the copper catalyst requires high overpotential (~ -1.0 V vs. RHE) and suffers from poor selectivity due to the concurrent occurrence of the hydrogen evolution reaction (HER).[6]

Several strategies have been proposed to suppress HER and direct the reduction current to hydrocarbons on Cu by altering experimental parameters,[7] such as working potential,[6, 8] pH,[9] pressure,[10] and temperature.[11] In the perspective of temperature, Hori et al. firstly reported reduced Faradaic efficiency (FE) for H_2, C_2H_4, and CO and increased FE for CH_4 with decreasing temperature from 40^{o}C to 0^{o}C.[12] Recently, Ahn et al. performed CO_2RR on Cu in the temperature range from 2^{o}C to 42^{o}C and showed that lower temperatures could increase the current efficiency of CH_4 and suppress HER.[13] However, they reported no obvious trend for C_2H_4 and CO with changing temperature. It is important to note that Hori et al. and Ahn et al. studied the CO_2RR under different experimental conditions (-1.56 V vs. RHE in 0.5 M $KHCO_3$ in the former, -1.00 V vs. RHE in 0.1M $KHCO_3$ in the latter). Therefore, it is difficult to use these findings to do a comparative analysis of the temperature dependence. Besides, the temperature effect at low overpotentials is also missing.

In this study, we report our measurement of the temperature dependent CO_2RR on Cu across a range of overpotentials for major gaseous products: CH_4, C_2H_4, CO, and H_2. In addition

to analyzing the selectivity shift through factors such as the concentration of CO_2, we explain from a reaction-energy landscape perspective, which consists of the relation between activation barrier (E_a) and the overpotentials for each product. The advancement of the understanding of the CO_2RR theory behind the temperature effect may enable new CO_2RR catalyst development in the future.

II. Experimental Methods

A. Copper Working Electrode Preparation

Polycrystalline copper foil (BTC, 0.1mm thick, 99,9999%) was cut into 0.5 cm × 0.5 cm pieces for preparation of the working electrode. A titanium wire was attached to each copper piece with Leitsilber 200 Silver Paint (Ted Pella, Inc.) and dried for at least two hours. After, both the copper foil and part of the titanium wire were covered by inert epoxy (Omegabond 101) except the 0.1 cm^2 test area and dried overnight. Before each experiment, the copper electrode was electropolished in 85% phosphoric acid (Sigma Aldrich) for 1 s at 1 $A \cdot cm^{-2}$ and rinsed thoroughly by 18.2 mΩ deionized water.[14]

B. Electrochemical Characterization

A custom glass H-Cell with water circulation jackets was designed for the temperature-dependent experiment based on previous CO_2RR studies. A Nafion® 117 membrane was used to separate the catholyte and anolyte chambers, which held 15 mL and 7 mL 0.1 M $KHCO_3$ electrolyte respectively. CO_2 (Airgas, ultra-high purity) gas was bubbled into catholyte inner chamber for about 20 min at 20 $mL \cdot min^{-1}$ flow rate before each measurement and at 1 $mL \cdot min^{-1}$ during the experiment.

A Bio-Logic SP-300 potentiostat was used for the electrochemical characterization with a conventional three-electrode system, in which the counter electrode is platinum wire placed into anolyte chamber, and the reference electrode is Ag/AgCl set in the catholyte chamber along with

the copper working electrode. The potentiostat compensated 85% of the uncompensated resistance (Ru). The remaining 15% was post-corrected to obtain the iR-corrected potential. The Ag/AgCl reference electrode was calibrated by measuring the onset voltage of hydrogen evolution/oxidation current on a polycrystalline platinum disk (Pine) in hydrogen (Airgas, ultra-high purity) saturated 0.1 M $KHCO_3$ to obtain reversible hydrogen electrode (RHE) at each temperature. We measured 0 V vs RHE as -616 mV vs. Ag/AgCl at 5ºC, -609 mV vs. Ag/AgCl at 15ºC, -601 mV at 25 ºC, -593 mV at 35ºC, and -584 mV at 45ºC.

During the experiment, the outer jacket of the cell was connected to a refrigerated and heating circulator (Julabo, Model F25-ME) to let the temperature-controlled water circulate to maintain the desired experimental temperature in the inner chamber. The inner chamber was directly coupled to the gas chromatograph (GC) through the gas outlet with the rubber stopper capped at the top opening. The inner chamber temperature was monitored via a temperature sensor connected to the circulator after each experiment, and the temperature difference compared to the internal sensor was less than 0.5ºC.

C. Product Quantification

A GC (SRI Instruments Multiple Gas Analyzer #5) with a thermal conductivity detector (TCD) and flame ionization detector (FID) with argon (Airgas, ultra-high purity) as carrier gas was used to determine the quantity of the gas product. A hydrogen generator (H_2-100, SRI Instruments) was used for the FID carrier production. Gas was sampled from the reaction vessel 20 min after applying the overpotential, which spent 20 min to separate through the GC columns and a 10 min rest was applied to flush the GC. Over the 20-minute separation period, CH_4 was quantified as product concentration at 3.62 min and 10.07 min, CO and C_2H_4 at 5.47 min and 12.49 min respectively. There were two samples subsequently measured in 30 min interval so that the

total experimental time was 1 hour for each copper working electrode. The FE was calculated by dividing the number of charges required to produce the amount of each product by the total charge transferred during the time of the GC sampling. We reproduced the measurements three times, represented through the standard deviations in the obtained results.

III. Results and Discussion

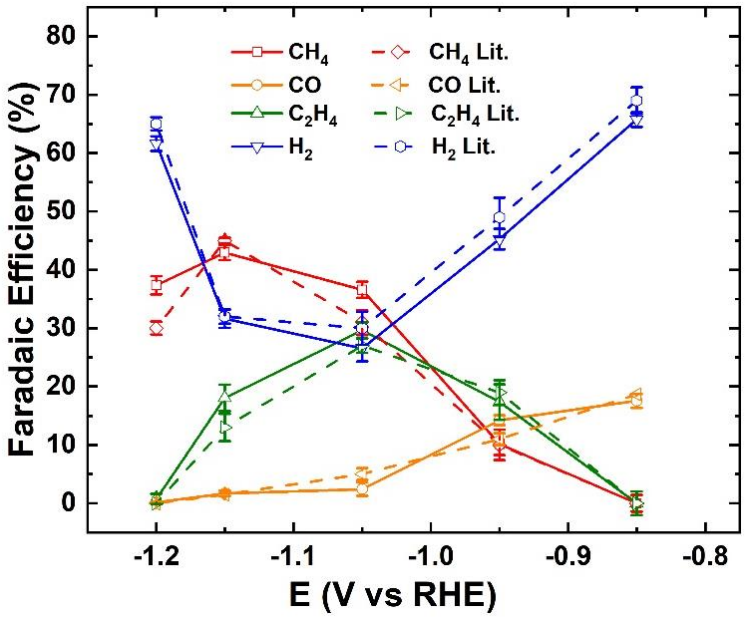

Figure 1. Cu CO_2RR with Designed Temperature Cell Compared to Literature[15] (Lit.) in CO_2 saturated 0.1M $KHCO_3$ at 25°C.

To ensure the working of the electrochemical cell, we firstly performed CO_2RR under room temperature (25°C) with a potential range between -0.85 V to -1.20 V vs. RHE. Figure 1 shows the results for the temperature-dependent cell, which is consistent with previously reported literature.[15] Then, we proceeded to other temperatures, 5°C, 15°C, 35°C, and 45°C to observe the change in selectivity by analyzing the composition of gaseous products CH_4, CO, C_2H_4, and H_2 via GC.

Figure 2a-d illustrates the FE for 5°C, 15°C, 35°C, and 45°C respectively. The FE for the HER decreases at lower temperatures for all potentials. The selectivity shifts to CH_4 with decreasing temperature. Remarkably, at 5°C, the CH_4 FE approaches to a FE of 60.5% at -1.20 V vs. RHE compared to 37.35% at 25°C. In contrast, HER dominates the product distribution at higher temperature. At 45°C, the FE of H_2 is greater than 55% at all potentials, whereas the CH_4 FE is smaller than 20%. The selectivity is slightly more favorable to CO under 35°C and 45°C in comparison to lower temperatures at more negative overpotentials (> -1.05 V vs. RHE). The temperature effect on the C_2H_4 selectivity is not obvious.

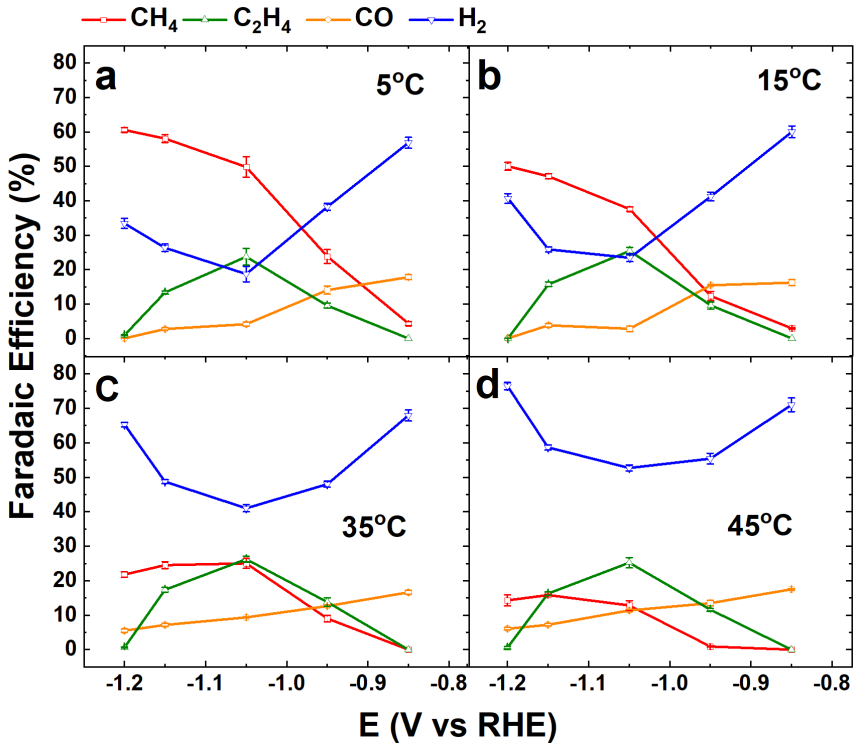

Figure 2. Faradaic efficiency for major gaseous products as a function of overpotentials (E) under a) 5°C. b) 15°C. c) 35°C. d) 45°C in CO_2 saturated 0.1M $KHCO_3$.

Several research groups have reported that the solubility of CO_2 in aqueous solution can significantly decrease with increasing temperature.[16, 17] We speculate that the CO_2RR selectivity suffers from the reduced CO_2 availability in the solution at higher temperatures (35°C and 45°C). In contrary, solubilized CO_2 is more available at lower temperatures (5°C, 15°C, and 25°C) to produce carbon products, such as CH_4. However, the slightly increasing current efficiency for CO at higher temperatures (35°C and 45°C) and the almost unchanged FE for C_2H_4 are straightforward to explain. Therefore, a more detailed analysis is essential.

Firstly, we conducted an Arrhenius analysis to quantify the effect of temperature by plotting the logarithm of the current density as a function of inverse temperature for each product. The total current density was obtained by averaging the Faradic current over the 1-hour experimental period and normalized by the electrode area, which can be subsequently multiplied by FE of each product to get the corresponding current density. Figure 3a-d shows the Arrhenius plots for CH_4, C_2H_4, CO, and H_2. For each product, we plotted at four fixed potentials -0.95, -1.05, -1.15, -1.20V vs. RHE. We applied a linear fit to each line according to the logarithm format of the Arrhenius equation:

$$\ln(\mathrm{i}) = -\frac{\mathrm{E_a}}{\mathrm{R}}\left(\frac{1}{\mathrm{T}}\right) + \ln(\mathrm{A}) \qquad \textbf{(1)}$$

where E_a is the activation energy, and A is the pre-exponential factor.[18]

From the values of E_a displayed on Figure 3, the activation barrier of CH_4 decreases with increasing overpotentials, indicating that that the application of overpotential can reduce the activation barrier toward the CH_4 production. This observation is consistent with Figure 2, which shows that the current efficiency toward CH_4 increases with potential regardless of the temperature (except for a slight decrease at -1.20V at 25°C in Figure 1). In comparison, CO shows an increasing E_a with potential, which is consistent with the observed selectivity suppression with increasing

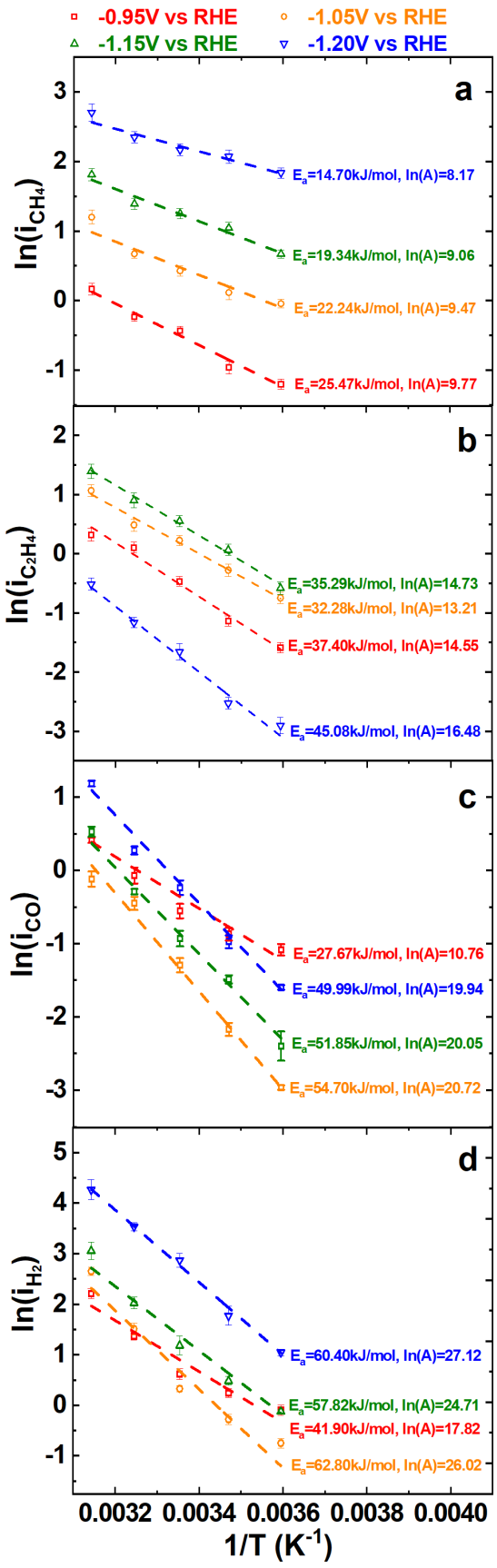

potentials. The similar case shows for C_2H_4. The selectivity is most favorable at -1.05V given the smallest activation barrier, whereas the largest E_a at more negative potentials, -1.15V and -1.20V vs RHE, where the C_2H_4 FE is highly suppressed. Interestingly, the activation barrier of H_2 is consistently the highest and H_2 therefore has the largest value of ln(A), despite being one of the most common CO_2RR product. This observation implies that HER likely occurs on the majority of the sites, in comparison to hydrocarbons that require special sites for catalysis, as stated in literatures that CH_4 production is observed at Cu (211)[19] and Cu (111)[20], and C_2H_4 at Cu (100) and Cu (111) face.[21]

Figure 3. Arrhenius Plots for a) CH_4, b) C_2H_4, c) CO, d) H_2 at the overpotentials: -0.95V, -1.05V, -1.15V, and -1.20V vs RHE. Activation energy, E_a, and logarithm of pre-exponential factor, ln(A), were labeled with the corresponding fitted lines.

We can plot E_a vs potentials (E) (Figure 4) to reveal the relationship between the reaction kinetics and the electrochemical potential driving force. CH_4 expresses a linear relationship between E_a and potential. We, therefore, apply the Butler-Volmer equation as a first approximation to explain the mechanism behind the CH_4 production as Butler-Volmer equation is a derivation of Arrhenius equation[22]. We assume that the overpotential, $\eta = E - E_0$, is significant such that we can neglect the backward term:

Arrhenius equation: $$\ln(i) = -\frac{E_a}{R}\left(\frac{1}{T}\right) + \ln(A) \quad (1)$$

Butler-Volmer equation: $$\ln(i) = -\frac{\alpha F}{R}\left(\frac{1}{T}\right) \cdot E + \ln(i_0) \quad (2)$$

Since each equation consists of a temperature related term and a constant, the two temperature related terms could be set equal as:

$$-\frac{E_a}{R}\left(\frac{1}{T}\right) = -\frac{\alpha F}{R}\left(\frac{1}{T}\right)\eta \quad (3)$$

Therefore, we could obtain a linear relation between E_a and E with a slope, dependent on the charge transfer coefficient, α, an indicator of the surface species coverage:[23]

$$E_a = \alpha F \cdot E \quad (4)$$

In Figure 4, as the linear relation between E_a and E is off at more negative overpotentials for CH_4, α is extrapolated separately as α_1=0.96 in the range of potentials from -1.15V to -1.20V vs RHE and α_2=0.32 for -0.95 to -1.15 V vs RHE according to Equation (4). The Butler-Volmer relation is plotted in Figure 5 so that another α can be derived based on Equation (2) as α=0.25 to 0.29 under different temperatures, which is close to the value of α=0.32 from the E_a vs E approach at less negative potentials. Therefore, the pathway of CH_4 production could be analogous to a simple

Butler-Volmer relation while the reaction potential falls between -0.95V and -1.15V vs RHE. At more negative overpotentials (E<-1.15V vs RHE), the larger α (=0.96) could imply an increasing CH_4 intermediate coverage at Cu surface during the reaction, which may lead to different reaction kinetics and thus a different pathway for CH_4 production.

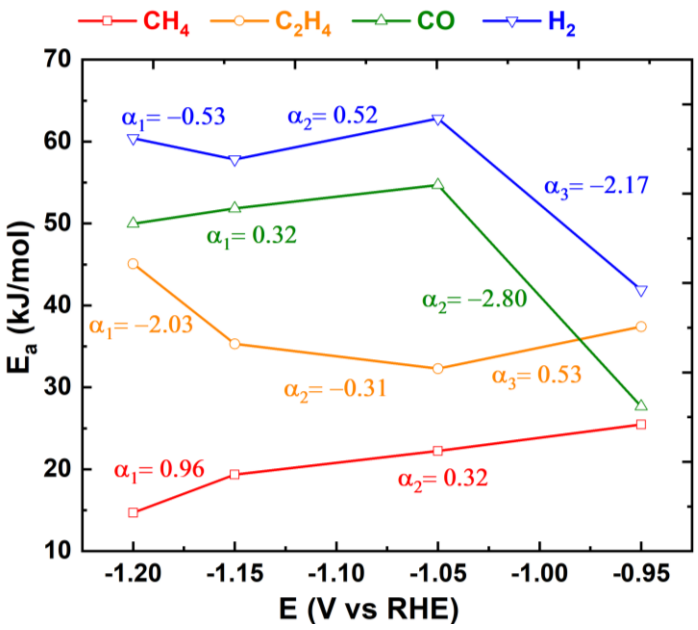

Figure 4. E_a vs. potential (E) for major gaseous products. Charge transfer coefficient, α, is labeled for each linear region.

Even though other gaseous products, C_2H_4, CO, and H_2, do not have a linear relation between E_a and E, the obviously changing α with the potential may indicate a significant alteration in the surface coverage. In the potential range of -0.95 to -1.05 V vs RHE, the very negative α for H_2 (α_3=-2.17) and CO (α_3=-2.80) implies that the surface species to produce H_2 and CO are highly reduced. These findings may suggest that H_2 species are consumed for the protonation of CO, a major intermediate of CO_2RR, to produce hydrocarbons, CH_4 and C_2H_4, which is consistent with the observations in Figure 1 and 2 that at each temperature,

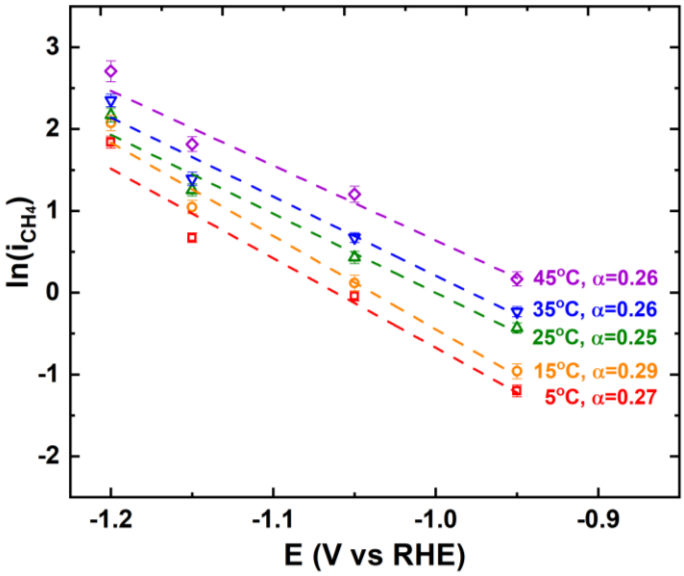

Figure 5. Butler-Volmer fitting for CH_4 at each temperature. Charge transfer coefficient, α, is labeled for each line.

the FE of hydrocarbons increased from -0.95 to -1.05 V vs RHE, but that of H_2 and CO was suppressed. At more negative potentials, -1.15 to -1.20 V vs RHE, the charge transfer coefficient is also negative (α_1=-0.53) for H_2 because it keeps converting to CH_4 via protonation at lower temperatures (5 ^oC and 15 ^oC). However, the α of CO maintains positive as the FE is slightly increasing at higher temperatures (35 ^oC and 45 ^oC). We hypothesize that there might be additional energy barriers for CO conversion to hydrocarbons as an intermediate with increasing temperature under high overpotentials.

Literatures have introduced two major pathways for C_2H_4 with one about the protonation of CO, sharing the intermediate (Cu bound CHO) which also produces CH_4 on Cu (111)[19, 24] and another involving in a CO dimer (adsorbed C_2O_2) as a key intermediate on Cu (100)[21, 25]. In Figure 4, α is positive (α_3=0.53) and larger than that of CH_4 (α_2=0.32) from -0.95 to -1.05 V vs RHE, indicating that the surface coverage of C_2H_4 species is greater than CH_4. This observation may suggest that the protonation pathway is preferential to produce C_2H_4 rather than CH_4 at less negative potentials, as in Figure 1 and 2, the selectivity is favorable for C_2H_4 over CH_4 at -0.95V vs RHE at 25, 35 and 45 ^oC. Under lower temperatures, such as 5 and 15^oC, since there are excess H_2 species available (H_2 is suppressed) to generate hydrocarbons, the reduction current gradually produces more CH_4 because of its low activation energy barrier. When the overpotential is below -1.05V vs RHE, α becomes more and more negative possibly because the protonation pathway shifts to CH_4 production at more negative potentials, implying a decreasing surface C_2H_4 species concentrations during the reaction. This finding is in well agreement with every temperature that C_2H_4 starts to be suppressed from -1.15V, and the FE is about 0 at -1.20V. In addition, it should be noted that the FE of C_2H_4 at each potential is almost not affected by changing temperature. We firstly assume that the protonation for C_2H_4 production may not be significantly influenced by

temperature. However, since there are limited H_2 species (far more amount of H_2 is produced instead) available for the protonation while increasing temperature, the CO dimerization pathway may play an important role at high temperatures upon the C_2H_4 production.

IV. Conclusion

We have shown that decreasing temperature can suppress HER and increase the CO_2RR selectivity toward CH_4 from less negative overpotentials, -0.95V vs RHE, to highly negative overpotentials, -1.20V vs RHE. According to the Arrhenius equation and consequent E_a vs E analysis, we hypothesize that the mechanism of CH_4 production could be analogous to Butler-Volmer pathway in the potential range from -0.95V to -1.05V. The coverage of the H_2 surface species is reduced to protonate the intermediate CO to produce hydrocarbons, and CH_4 is more favorable than C_2H_4 when the overpotential is below -1.05V. Because there is no adequate H_2 species for the protonation of CO at higher temperatures (35 and 45^{o}C), the CO dimerization pathway may contribute the stable FE of C_2H_4 when the temperature is increasing. With such fundamental analysis of the complicated temperature dependent CO_2RR on Cu, our work points to a potential method to understand the reaction rates and mechanism pathways from the perspective of the activation barrier. The temperature dependent technique and the activation energy analysis could be adapted to other catalytic materials in the future research.

V. REFERENCES

1. Cline, W.R. The economics of global warming. *Energy Studies Review* **1992**, *4*, 307-310.
2. Kondratenko E.V.; Mul G.; Baltrusaitis, J.; Larrazábal, G.O.; Pérez-Ramírez, J. Status and perspectives of CO_2 conversion into fuels and chemicals by catalytic, photocatalytic and electrocatalytic processes. *Energy Environ. Sci.* **2013**, *6*, 3112-3135.
3. Delacourt, C.; Ridgway, P.L.; Kerr, J.B.; Newman, J. Design of an Electrochemical Cell Making Syngas ($CO + H_2$) from CO_2 and H_2O Reduction at Room Temperature. *J. Electrochem. Soc.* **2008**, *155*, B42.
4. Hori, Y.; Murata, A.; Takahashi, R. Formation of hydrocarbons in the electrochemical reduction of carbon dioxide at a copper electrode in aqueous solution. *J. Chem. Soc. Faraday Trans. 1* **1989**, *85*, 2309-2326.
5. Gattrell, M.; Gupta, N.; Co, A. Electrochemical reduction of CO_2 to hydrocarbons to store renewable electrical energy and upgrade biogas. *Energy Convers. Manage.* **2007**, *48*, 1255-1265.
6. Kuhl, K.P.; Cave, E.R.; Abram, D.N.; Jaramillo, T.F. New insights into the electrochemical reduction of carbon dioxide on metallic copper surfaces. *Energy Environ. Sci.* **2012**, *5*, 7050.
7. Gattrell, M.; Gupta, N.; Co, A. A review of the aqueous electrochemical reduction of CO_2 to hydrocarbons at copper. *J. Electroanal. Chem.* **2006**, *594*, 1-19.
8. Li W.C.; Kanan, M.W. CO_2 reduction at low overpotential on Cu electrodes resulting from the reduction of thick Cu_2O films. *J. Am. Chem. Soc.* **2012**, *134*, 7231-7234.
9. Varela, A.S.; Kroschel, M.; Reier, T.; Strasser, P. Controlling the selectivity of CO2 electroreduction on copper: The effect of the electrolyte concentration and the importance of the local pH. *Catal. Today* **2016**, *260*, 8-13.

10. Hara, K.; Tsuneto, A.; Kudo, A.; Sakata, T. Electrochemical reduction of carbon dioxide under high pressure on various electrodes in an aqueous electrolyte. *J. Electroanal. Chem.* **1995**, *391*, 141-147.
11. Azuma, M.; Hashimoto, K.; Hiramoto, M.; Watanabe, M.; Sakata, T. Electrochemical reduction of carbon dioxide on various metal electrodes in low-aemperature Aqueous $KHCO_3$ Media. *J. Electrochem. Soc.* **1990**, *137*, 1772-1778.
12. Hori, Y.; Kikuchi, K.; Murata, A.; Suzuki, S. Production of methane and ethylene in electrochemical reduction of carbon dioxide at copper electrode in aqueous hydrogencarbonate solution. *Chem. Lett.* **1986**, 897-898.
13. Ahn, S.T.; Abu-Baker, I.; Palmore, G.R. Electroreduction of CO_2 on polycrystalline copper: Effect of temperature on product selectivity. *Catal. Today* **2017**, *288*, 24-29.
14. Hori, Y.; Konishi, H.; Futamura, T.; Murata, A.; Koga, O.; Sakurai, H.; Oguma, K. "Deactivation of copper electrode" in electrochemical reduction of CO_2. *Electrochim. Acta* **2005**, *50*, 5354-5369.
15. Kimura, K.W.; Fritz, K.E.; Kim, J.; Suntivich, J.; Abruña, H.D.; Hanrath, T. Controlled selectivity of CO_2 reduction on copper by pulsing the electrochemical potential. *ChemSucChem* **2018**, *11*, 1781-1786.
16. Zhong, H.; Fujii, K.; Nakano, Y. Electroactive species in the electrochemical reduction of CO_2 in $KHCO_3$ solution at elevated temperature. *J. Energy. Chem.* **2016**, *25*, 517-522.
17. Jesús, H.D.; Moral C.D.; Cabrera, C. R. Voltammetric study of CO_2 reduction at Cu electrodes under different $KHCO_3$ concentrations, temperatures and CO_2 pressures. *J. Electroanal. Chem.* **2001**, *513*, 45-51.
18. Logan, S.R. The origin and status of the Arrhenius equation. *J Chem Educ.* **1982**, *59*, 279-281.

19. Peterson, A.A.; Abild-Pedersen, F.; Studt, F.; Rossmeisl, J.; Norskov, J.K. How copper catalyzes the electroreduction of carbon dioxide into hydrocarbon fuels. *Energy Environ. Sci.* **2010**, *3*, 1311-1315.
20. Nie, X.; Espoi, M.R.; Janik, M.J.; Asthagiri, A. Selectivity of CO_2 reduction on copper electrodes: The role of the kinetics of elementary steps. *Angew. Chem. Int. Ed.* **2013**, *52*, 2459-2462.
21. Schouten K.J.P.; Qin, Z.; Gallent, P.Z.; Koper, M.T.M. Two pathways for the formation of ethylene in CO reduction on single-crystal copper electrodes. *J. Am. Chem. Soc.* **2012**, *134*, 9864-9867.
22. Hulett, J.R. Derivations from the Arrhenius equation. *Q. Rev. Chem. Soc.* **1964**, *18*, 227-242.
23. Kornyshev, A.A.; Schmickler, W. On the coverage dependence of the partial charge transfer coefficient. *J Electroanal. Chem.* **1986**, *202*, 1-21.
24. Montoya, J.H.; Peterson, A.A.; Norskov, J.K. Insights into C-C coupling in CO_2 electroreduction on eopper Electrodes. *ChemCatChem* **2013**, *5*, 737-742.
25. Calle-Vallejo, F.; Koper M.T.M. Theoretical considerations on the electroreduction of CO to C_2 species on Cu(100) electrodes. *Angew. Chem. Intl. Ed.* **2013**, *52*, 7282-7285.

VOLUME II: TEMPERATURE DEPENDENT ELECTROCHEMICAL CO_2 REDUCTION REACTION ON MANGANESE OXIDE

I. Introduction

Colloidal nanocrystals (NCs) have been a very popular field in the materials research as notable high-performance and low-cost energy conversion catalysts.[1] For this reason, we selected manganese oxide (Mn_3O_4) as a candidate to investigate electrochemical CO_2 reduction (CO_2RR) as well as the temperature dependent experiment upon understanding the underlying mechanism on copper. However, current NCs syntheses mostly require metal binding surfactants, such as ligands, to control the particle solubility, growth rates and relative surface energies.[2, 3] For the electrochemical catalysis, in this thesis, CO_2RR, the ligands must be removed as otherwise they could hinder the catalyst performance.

In this volume, we compare four ligand-removal treatments of Mn_3O_4 NCs, denoted as heat, alkylating, Lewis-acid, and base (Figure 1). All Mn_3O_4 NCs samples were synthesized and physically characterized by our collaborator Andrew Nelson from Professor Richard Robinson Group at Cornell University. Our work mainly focused on the electrochemical characterization by firstly evaluating the electrochemical surface through the cyclic voltammetry (CV). Then, each sample was analyzed by performing CO_2RR under different temperatures with the same manner as Volume I. By comparing the electrochemically active surface area (ECSA) and the CO_2RR activity of each ligand-removal sample, the most efficient ligand-removal method could be concluded, and the mechanism in Volume I may also be approved by the temperature dependent CO_2RR experiment on a set of catalysts other than coo

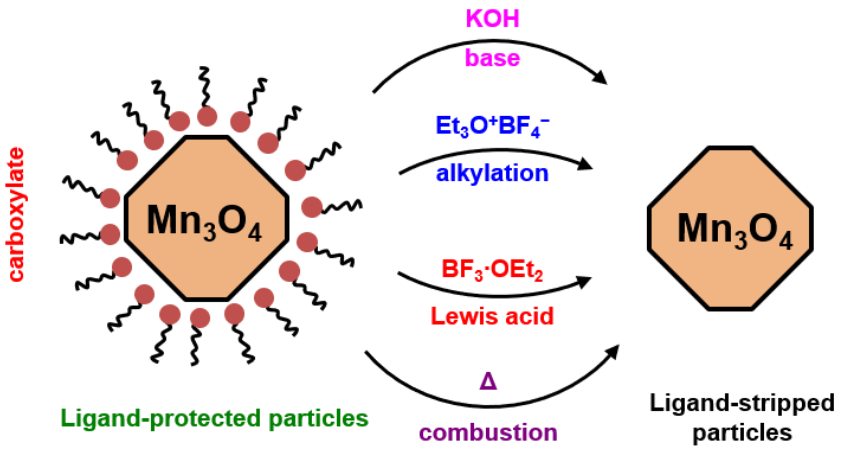

Figure 1. Schematic diagram of ligand-removal treatment for Mn3O4 NCs: thermal, alkylation, Lewis-acid, and base treatment (figure from our recent published work). [4]

II. Experimental Methods

A. Synthesis of Mn_3O_4 and Ligand-removal Samples

Mn_3O_4 NCs were synthesized by adding water to manganese acetate with oleylamine and oleic acid in xylene, so that the passivated surface ligand was carboxylate group (COO^-) from oleylamine.[5] The thermal treatment was done by combusting Mn_3O_4 NCs in air for 1 hour at 300°C.[6] In the alkylation method, an alkylating agent, triethyloxonium tetrafluoroborate (Et_3OBF_4), was used to strip the COO^- ligands at NCs surface by esterification.[7] The Lewis-acid treatment is generally a typical acid-base reaction between boron trifluoride (Et_2OBF_3, a Lewis acid) and the Lewis-basic carboxylate ligands.[8] In the last method, base treatment, the ligand can be abstracted by a metathesis reaction between the carboxyl groups and an inorganic base, in Andrew's case, potassium hydroxide (KOH).[9, 10]

The detailed synthesis procedures of Mn_3O_4 NCs and the subsequent ligand-removal samples can be referred to the paper we collaboratively published with Robinson Group recently,[4] and our work was on the following electrochemical experiment.

B. Electrochemical Characterization

Catalyst inks were prepared by dispersing 3mg of Mn_3O_4/C (Mn_3O_4:C=1:1 by mass) composites in 2948.52 μL isopropanol/water (1:4 by volume, carrier) with addition of 51.48 μL of 0.1M aqueous KOH neutralized Nafion® 117 solution as a binder to an ink concentration of 0.5 mg_{Mn3O4} mL^{-1}. The ink was then sonicated for 10 minutes using a probe sonicator. Subsequently, to improve the reproducibility of the cyclic voltammograms, the concentrated ink was diluted by adding carrier to a final ink composition of 0.15 mg_{Mn3O4} mL^{-1}, 0.15 mg_{carbon} mL^{-1}, 0.3 mg_{Nafion} mL^{-1}. The diluted ink was dispersed using a probe sonicator for 10 minutes, and 10L was deposited on a glassy carbon electrode (GCE, disk area=0.196cm^2). The film was dried under a downward 500mL beaker consisting of an upturned beaker containing an open vial of isopropanol to increase the alcohol vapor pressure in the chamber.

A Bio-Logic SP-300 potentiostat was used with a traditional three electrode cell (Pine Research Instrumentation) for all electrochemical characterization. The counter electrode was a platinum wire, while an Ag/AgCl reference electrode (Pine) was used with 0.1 M KOH as the supporting electrolyte. All reported potentials are referenced to the reversible hydrogen electrode (RHE) scale which was calibrated by measuring the onset voltage of hydrogen evolution/oxidation current on a polycrystalline platinum disk (Pine) in hydrogen (Airgas, ultra-high purity) saturated 0.1 M KOH. Using this approach, we measured 0V vs RHE to be -0.9807V vs Ag/AgCl. All CV measurements on the Mn_3O_4/C composites were conducted in 0.1 M KOH saturated with argon (Airgas, ultra-high purity) at a scan rate of 50 mV/s. The ECSA was calculated by subtracting the double-layer capacitance region from the cyclic voltammograms. Since the double-layer capacitance slightly increases with voltage, two sloped lines were used to fit the double-layer region boundaries, and the ECSA was finally integrated based on the sloped lines.

The experimental setup and conditions of CO_2RR were about the same as what we have used in the "Experimental Method" part of the Volume I except the working electrode. In this volume, a titanium wire was attached to a piece of glassy carbon with Leitsilber 200 Silver Paint (Ted Pella, Inc.) and dried for two hours. After that, both the copper foil and part of the titanium wire were covered by inert epoxy (Omegabond 101) except the ~0.2cm^2 test area (close to the area of GCE used for CV) and dried overnight. In each experiment, 10μL of 0.5 mg_{Mn3O4} mL^{-1} ink was deposited onto the working electrode test area to observe obvious electrochemical catalytic performance. The ink film was dried as the way in the previous CV part.

We tested each sample under 5^oC, 25^oC, and 35^oC. The temperature of the electrolyte was not raised up to 45^oC as copper because the ink stripped from the working electrode with increasing temperature.

III. Results and Discussion

Transmission electronic microscopy (TEM) was used to observe the particle morphology before and after the ligand-removal treatment. Figure 2a shows distinguishable Mn_3O_4 NCs, and there is no shape and little particle size change after each treatment, indicating that the morphology was stable.

As the particle morphology is unchanged, in the next step, all samples were examined the stability of the crystal structure by selected area electron diffraction (SAED) in case there would be a phase change after the ligand-removal treatment. Figure 2b demonstrates that the SAED patterns of all the Mn3O4 NCs agree well with the tetragonal Mn_3O_4 hausmannite structure (JCPDS 01-074-6605). Since there is no peak shift for all treated Mn_3O_4 NCs, the crystal phase is

stable with all ligand-removal methods. Therefore, we proceeded to perform electrochemical characterizations.

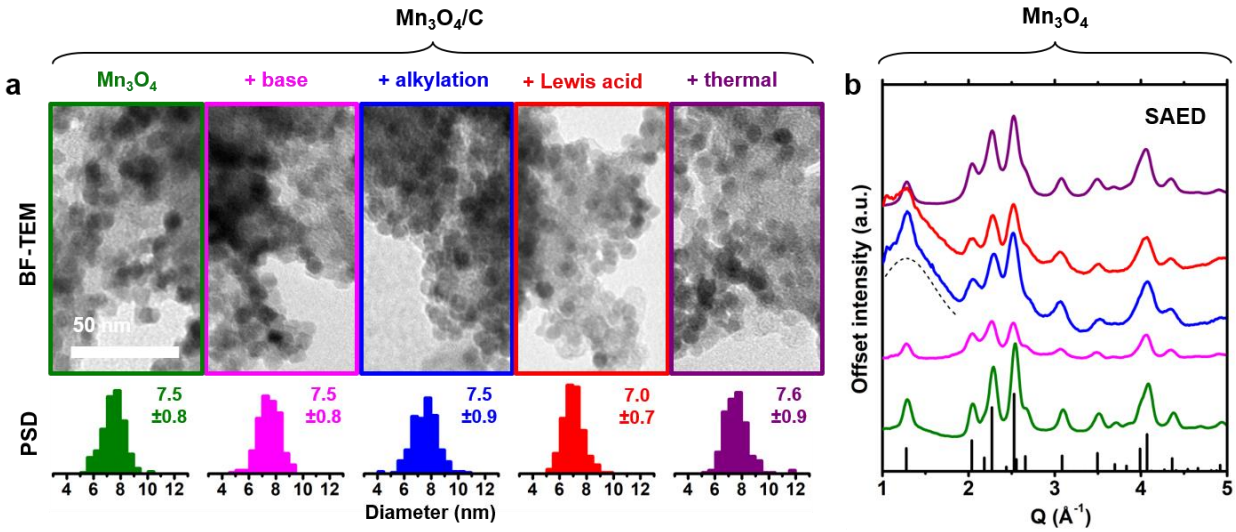

Figure 2. a) Figures of NCs in bright field TEM (BF-TEM, top) along with particle size distribution of the particle diameters (bottom) **b)** SAED patterns of NCs in well agreement with Mn_3O_4 phase for both untreated and treated samples (figure from our recent published work).[4]

Figure 3 shows the CV results for each ligand-removal sample. Three independent measurements are illustrated to show the reproducibility for each ligand-removal treatment. In general, two oxidation/reduction waves were observed at about 0.9 and 1.05V vs RHE,[11] representing the redox couple Mn^{3+}/Mn^{4+}.[12, 13] We use the comparison of these redox features to assess the efficacy of the ligand removal treatment. Specifically, we measure the integrated charge underneath the redox waves to determine the ECSA. We calculated the ECSA for all three independent measurements of each ligand-removal sample and computed the average and standard deviation (STD) to numerically prove the reproducibility. From the results in Table 1, the STD is less than 5%, indicating that the measurements are reproducible.

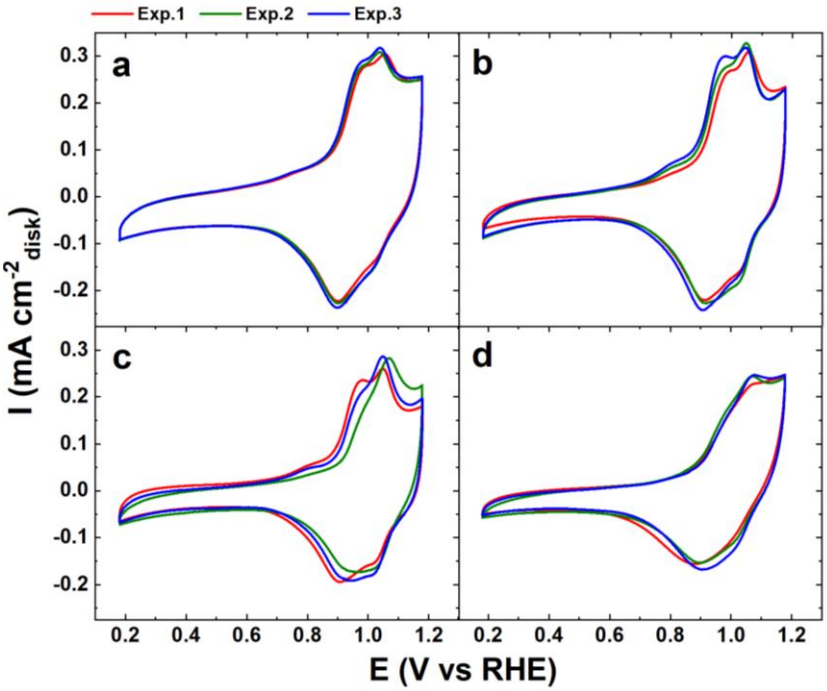

Figure 3. Cyclic voltammograms of **a)** thermal, **b)** alkylation, **c)** Lewis-acid, **d)** base treated Mn_3O_4 NCs in Ar saturated 0.1M KOH, with 50m/s scan rate. Three independent measurements are shown for each sample to illustrate the reproducibility.

To closely compare the average of ECSA for each ligand-removal treatment, the alkylation-treated Mn3O4 NCs demonstrate the largest ECSA and the best well-defined wave structures. The thermal treatment gives the second largest ECSA but the best reproducible redox peaks. These findings may suggest that the ligand detachment by esterification and air combustion has the potential to a clean surface for electrochemical applications. However, treatment with Lewis-acid produces Mn_3O_4 with similar cyclic voltammograms to those with alkylation or thermally treated Mn_3O_4, but the curves are less reproducible, as indicated by the varying shape of the wave structures. Also, the ESCA of the Lewis-acid treated sample is smaller. We hypothesize that the Lewis-acid treatment may produce more reactive degradation species, which could alter the surface redox properties of Mn_3O_4 NCs. In comparison, base treated Mn_3O_4 has the smallest

ECSA response and a less well-defined wave structure, implying that there might be less-accessible redox sites for electrochemical reactions.

	Method			
ECSA ($\mu C \cdot cm^{-2}$)	**Base**	**Alkylation**	**Lewis Acid**	**Thermal**
CV #1	771	1176	901	1066
CV #2	763	1197	929	1089
CV #3	778	1213	944	1114
Average	771	1195	925	1089
STD (%)	0.79	1.28	1.94	1.57

Table 1. ECSA derived from three independent CV measurements on Mn_3O_4/C nanocomposites for each ligand-removal method.

From the CV analysis, it could be supposed that the cleanest surfaces, alkylation or thermal treated samples, would result in most electrocatalytic efficiency. However, by firstly performing CO_2RR on treated Mn_3O_4 NCs under room temperature, all the reduction current contributed to HER at all potentials for each ligand-removal sample and there was even no evidence to show the cleanest ligand-removal surface for hydrogen production by only looking at the Faradaic Efficiency (FE) of H_2 in the results (Figure 4 a-d). Since in the Volume I, the current efficiency of CH_4 and H_2 can be significantly affected by temperature, we decided to perform temperature dependent CO_2RR to observe whether there would be any selectivity shift to help assess the ligand removal methods as well as discover a possible CO_2RR catalyst with unique performance by changing temperature.

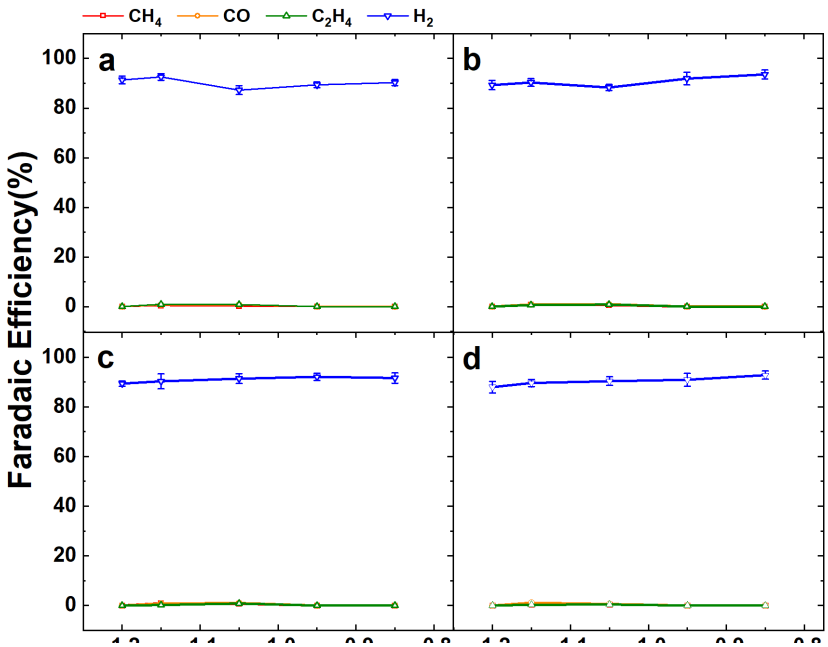

Figure 4. FE for major gaseous products as a function of overpotential (E). **a)** thermal, **b)** alkylation, **c)** Lewis-acid, **d)** base treated Mn_3O_4 NCs in CO_2 saturated 0.1M $KHCO_3$ at 25°C.

Unfortunately, both lower (5°C, Figure 5a-d) and higher temperatures (35°C, Figure 6a-d) did not show any selectivity shift to any hydrocarbon for any ligand-removal sample. Therefore, Mn_3O_4 may not be an efficient CO_2RR catalyst with the condition of only changing the temperature.

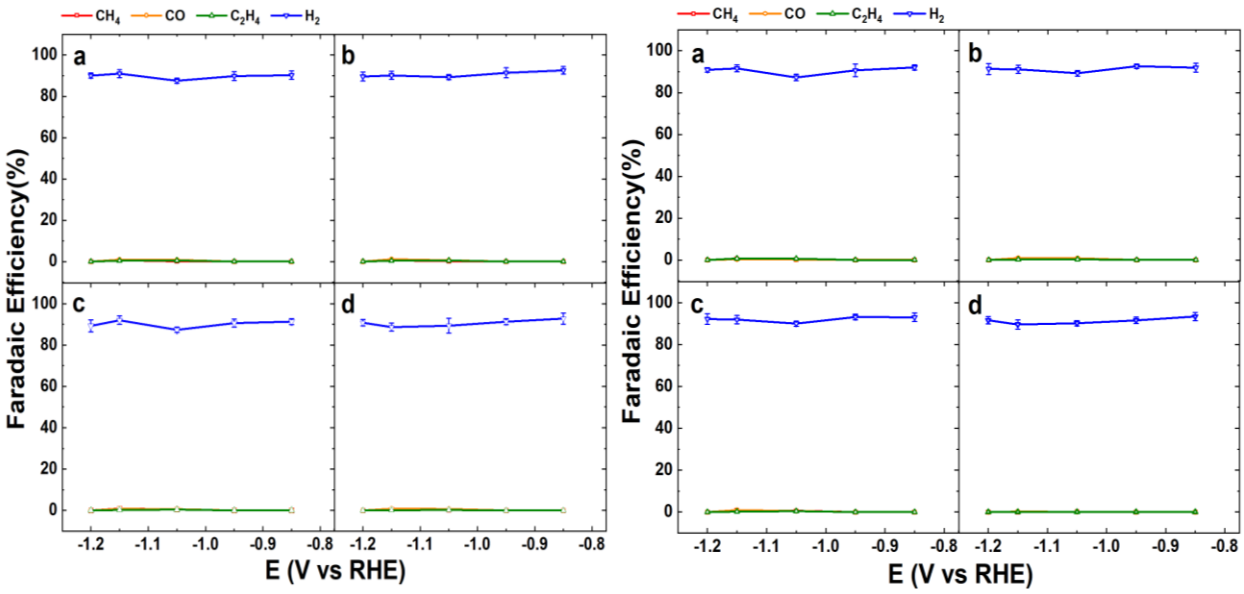

Figure 5. FE for major gaseous products as a function of overpotential (E). **a)** thermal, **b)** alkylation, **c)** Lewis-acid, **d)** base treated Mn_3O_4 NCs in CO_2 saturated 0.1M $KHCO_3$ at 5°C.

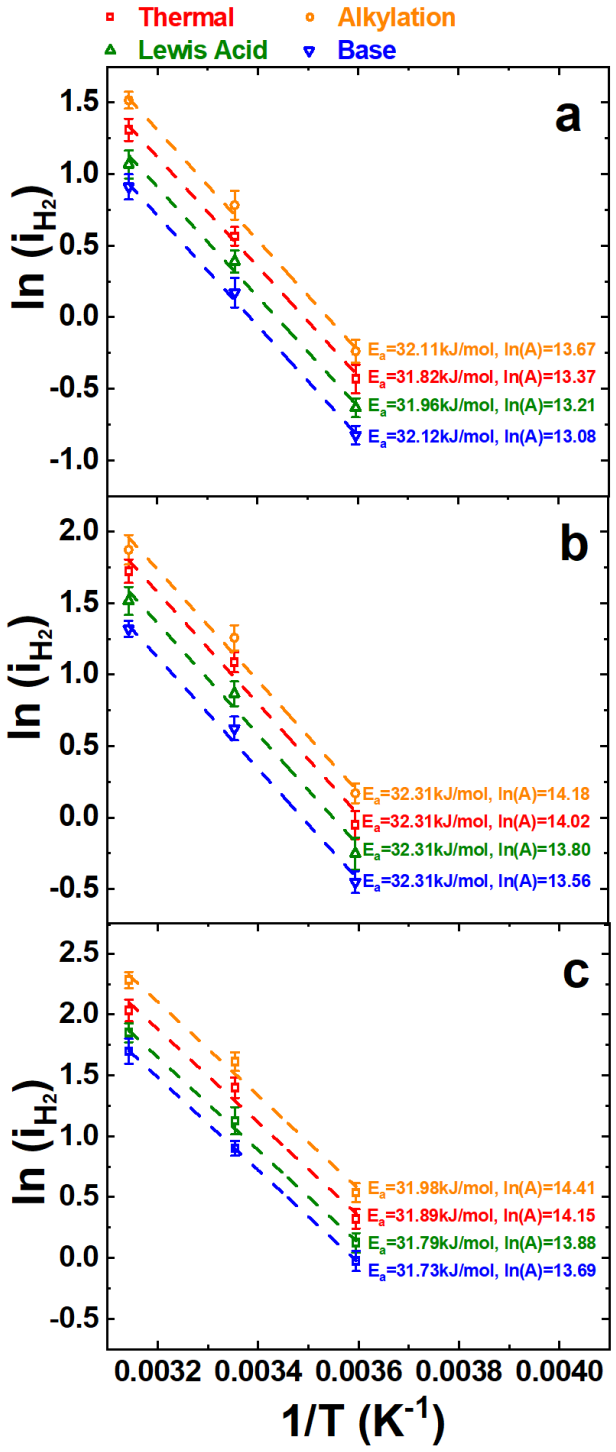

Figure 6. FE for major gaseous products as a function of overpotential (E). **a)** thermal, **b)** alkylation, **c)** Lewis-acid, **d)** base treated Mn_3O_4 NCs in CO_2 saturated 0.1M $KHCO_3$ at 35°C.

Nevertheless, the most efficient method to clean the catalyst surface can be assessed by analyzing Arrhenius plot using data from the temperature dependent experiment as we have already done in Volume 1 for copper. The Arrhenius plot for each ligand-removal sample at -0.95V vs RHE, -1.05V vs RHE, and -1.15V vs RHE is illustrated in Figure 7a-c. From these figures, the activation energy, E_a, is similar for each treated Mn_3O_4 NCs, which is as expected because the phase of Mn3O4 was not changed by the ligand-removal treatment (as examined by SAED in Figure 2b). However, at each potential, the logarithm of the pre-exponential factor, ln(A), shows alterations among different treated samples. Because A could be an indicator of the available surface area and diffusion rate at the nanocrystal surfaces in the Arrhenius equation,[14, 15] the alkylation treated Mn3O4 NCs with the largest value of ln(A) has the biggest area

Figure 7. Arrhenius plots for each ligand removal sample at **a)** -0.95V, **b)** -1.05V, **c)** -1.15V vs RHE. Activation energy, E_a, and logarithm of pre-exponential factor, ln(A), were labeled with the corresponding fitted lines.

available and highest surface diffusion rate so that can provide the most efficient and cleanest surface for catalysis during the reaction. The thermal treatment. The way of comparing ln(A) is consistent with the results from evaluating the ligand-removal efficiency by the reproducibility of the cyclic voltammograms and ECSA. Therefore, the alkylation treatment could be the most promising methods to clean the NCs surfaces for high electrochemical catalytic performance.

IV. Conclusion

In conclusion, we have electrochemically evaluated the ligand-removal strategies of the Mn_3O_4 NCs. For the purpose of discovering possible catalysts for CO_2RR, none of the treated Mn_3O_4 NCs were efficient for catalysis with all reduction current contributing to HER and had no selectivity shifted to hydrocarbons while changing temperatures. In future research, materials could be continuously discovered as potential CO_2RR catalysts and observed the change of the hydrocarbon production via temperature dependent measurements. Nonetheless, from the CV and Arrhenius analysis, the alkylation treatment can be concluded as the most promising method to clean the surface ligands because of the reproducible cyclic voltammograms and the largest ECSA as well as the biggest pre-exponential factor in the Arrhenius analysis. This alkylation method could have provided an insight for NCs surface cleaning with synthesis procedures, requiring binding surfactants.

V. RENERENCES

1. Yin, Y.; Alivisatos, A. P. Colloidal nanocrystal synthesis and the organic–inorganic interface. *Nature* **2005,** *437*, 664–670.
2. Jia, C.-J.; Schüth, F. Colloidal metal nanoparticles as a component of designed catalyst. *Phys. Chem. Chem. Phys.* **2011,** *13*, 2457-2487.
3. Boles, M. A.; Ling, D.; Hyeon, T.; Talapin, D. V. The surface science of nanocrystals. *Nat. Mater.* **2016,** *15*, 141-153.
4. Nelson, A.; Zong, Y., Fritz, K. E.; Suntivich, J.; Robinson, R. D. Assessment of soft ligand removal strategies: alkylation as a promising alternative to high-temperature treatments for colloidal nanoparticle surfaces. *ACS Mater. Lett.* **2019**, *1*, 177-184.
5. Yu, T.; Moon, J.; Park, J.; Park, Y. I.; Na, H. B.; Kim, B. H.; Song, I. C.; Moon, W. K.; Hyeon, T. Various-shaped uniform Mn_3O_4 nanocrystals synthesized at low temperature in air atmosphere. *Chem. Mater.* **2009,** *21*, 2272-2279.
6. Guo, S.; Zhang, S.; Wu, L.; Sun, S. Co/CoO nanoparticles assembled on graphene for electrochemical reduction of oxygen. *Angew. Chem. Int. Ed.* **2012,** *124*, 11940-11943.
7. Rosen, E. L.; Buonsanti, R.; Llordes, A.; Sawvel, A. M.; Milliron, D. J.; Helms, B. A. Exceptionally mild reactive stripping of native ligands from nanocrystal surfaces by using Meerwein's salt. *Angew. Chem., Int. Ed.* **2012,** *51*, 684-689.
8. Doris, S. E.; Lynch, J. J.; Li, C.; Wills, A. W.; Urban, J. J.; Helms, B. A. Mechanistic insight into the formation of cationic naked nanocrystals generated under equilibrium control. *J. Am. Chem. Soc.* **2014,** *136*, 15702-15710.

9. Nelson, A.; Fritz, K. E.; Honrao, S.; Hennig, R. G.; Robinson, R. D.; Suntivich, J. Increased activity in hydrogen evolution electrocatalysis for partial anionic substitution in cobalt oxysulfide nanoparticles. *J. Mater.Chem. A* **2016,** *4*, 2842-2848.
10. Zhang, H.; Hu, B.; Sun, L.; Hovden, R.; Wise, F. W.; Muller, D. A.; Robinson, R. D. Surfactant ligand removal and rational fabrication of inorganically connected quantum dots. *Nano Lett.* **2011,** *11*, 5356-5361.
11. Sheng, W.; Gasteiger, H. A.; Shao-Horn, Y. Hydrogen oxidation and evolution reaction kinetics on platinum: acid vs. alkaline electrolytes. *J. Electrochem. Soc.* **2010,** *157*, B1529-B1536.
12. Gorlin, Y.; Jaramillo, T. F. Investigation of surface oxidation processes on manganese oxide electrocatalysts using electrochemical methods and ex situ x-ray photoelectron spectroscopy. *J. Electrochem. Soc.* **2012,** *159*, H782-H786
13. McBreen, J. The electrochemistry of β-MnO_2 and γ-MnO_2 in alkaline electrolyte. *Electrochim. Acta* **1975,** *20*, 221-225.
14. Laidler, K. J. The development of Arrhenius equation. *J. Chem. Educ.* **1984**, *61*, 494-498.
15. Horvath, J.; Birringer, R.; Gleiter, H. Diffusion in nanocrystalline material. *Solid State Commun*. **1987**, *62*, 319-322.